Reduced Graphene Oxide–P25 Nanocomposites as Efficient Photocatalysts for Degradation of Bisphenol A in Water

Fei Yu [1], Xueting Bai [1], Changfu Yang [1], Lijie Xu [2],* and Jie Ma [3,4],*

[1] College of Marine Ecology and Environment, Shanghai Ocean University, No 999, Huchenghuan Road, Shanghai 201306, China

[2] College of Biology and the Environment, Nanjing Forestry University, Nanjing 210037, China

[3] Key Laboratory of Yangtze River Water Environment, College of Environmental Science and Engineering, Tongji University, Shanghai 200092, China

[4] Shanghai Institute of Pollution Control and Ecological Security, 1239 Siping Road, Shanghai 200092, China

*   Correspondence: xulijie@njfu.edu.cn (L.X.); jma@tongji.edu.cn (J.M.);
    Tel.: +86-15651721667 (L.X.); +86-021-6598-1831 (J.M.)

check for updates

Abstract: Reduced graphene oxide–titanium dioxide photocatalyst (rGO–TiO_2) was successfully synthesized by the hydrothermal method. The rGO–TiO_2 was used as photocatalyst for the degradation of bisphenol A (BPA), which is a typical endocrine disruptor of the environment. Characterization of photocatalysts and photocatalytic experiments under different conditions were performed for studying the structure and properties of photocatalysts. The characterization results showed that part of the anatase type TiO_2 was converted into rutile type TiO_2 after hydrothermal treatment and 1% rGO–P25 had the largest specific surface area (52.174 m^2/g). Photocatalytic experiments indicated that 1% rGO–P25 had the best catalytic effect, and the most suitable concentration was 0.5 g/L. When the solution pH was 5.98, the catalyst was the most active. Under visible light, the three photocatalytic mechanisms were ranked as follows: $O_2^{\bullet-} > \bullet OH > h^+$. 1% rGO–P25 also had strong photocatalytic activity in the photocatalytic degradation of BPA under sunlight irradiation. 1% rGO–P25 with 0.5 g/L may be a very promising photocatalyst with a variety of light sources, especially under sunlight for practical applications.

Keywords: photocatalysis; TiO_2; graphene; visible light; bisphenol A

1. Introduction

As a typical endocrine disruptor of the environment, bisphenol A (BPA) causes harm to the environment and human health because of the increasing concentrations in the environment [1]. Furthermore, it affects the physiological metabolism of higher animals [2]. At present, an advanced oxidation process (AOP), especially photocatalytic technology that uses semiconductor material as a catalyst, is widely applied in wastewater-treatment for BPA [3,4]. TiO_2 is one of the most effective photocatalysis for the decomposition of organic contaminants in water due to its merits of high activity, low cost, water insolubility, non-toxicity, and stable physical-chemical properties [3,5,6].

As currently known, when light irradiates the surface of TiO_2 with higher photo-energy than the bandgap of TiO_2, photoelectrons, and photo-holes will be generated. In sequence, electron-hole ($e^- $-$h^+$) pairs will be created, which provide the necessary material condition for the REDOX reaction [7,8]. These photoexcited electrons and holes have energy that can migrate freely. TiO_2 photocatalytic oxidation has the following advantages: strong oxidation ability, a much higher oxidation capacity of $\bullet OH$ than ordinary chemical oxidants [9]; low energy consumption, where the reaction can be carried

out under normal temperature and pressure [10]; modern production cleaning process, where the energy source of this process is solar energy that cannot cause secondary pollution, and organic matter can be mineralized into clean energy such as H_2O and CO_2 [11]; fast reaction rate, where organic pollutants can be destroyed completely within minutes to hours [12].

However, some drawbacks limit the practical application of TiO_2. For instance, fast h^+/e^- recombination [13]; the large bandgap energy of 3.2 eV can only be excited by ultraviolet light (UV) with a wavelength less than 387 nm [3,6,14–17]. In recent years, scientists have advanced many strategies in order to further improve the photocatalytic performance of TiO_2, such as doping with non-metallic elements, combining with metal ions, depositing noble metals, and creating heterojunctions with other semiconductors [12,18–22]. More recently, in contrast to other materials, graphene, graphene oxide (GO), and the graphene monolith formed by the stripping of GO, reduced graphene oxide (rGO) used in this experiment received wider attention because of its good mechanical strength, high electron mobility, chemical stability, optical properties, and high surface area [23–27]. Among them, rGO is a derivative of graphene and has a unique sp^2 hybrid carbon network [28]. The surface of the relatively inert graphene becomes extremely active due to the introduction of a large number of oxygen-containing functional groups such as hydroxyl group, epoxy group, carbonyl group, and a carboxyl group [29,30]. Therefore, the surface of graphene can also be connected to specific functions such as biomolecules, polymers, and inorganic particles [31]. The photocatalytic enhancement of rGO–TiO_2 composites can be attributed to three aspects: first, a large number of π–π conjugated double bonds are present on the graphene surface, so the organic molecules in the solution can be well enriched into graphene [32,33]. Therefore, the hydroxyl radicals and photogenerated holes generated by TiO_2 supported on the surface of graphene under ultraviolet light have a good degradation effect on organic matter [34,35]. Second, under the illumination of light, the photogenerated electrons and holes generated by anatase TiO_2 can be effectively separated, thereby suppressing carrier recombination [36–38]. Third, composite material solves the problem of large bandgap energy [4].

Using BPA as the target pollutant, the catalytic activity of 1% rGO–P25 photocatalyst under different conditions was studied, and the photocatalytic mechanism was compared. This work mainly solves the problem of the low efficiency of BPA degrading under the visible light of the TiO_2 photocatalyst, explores the optimal conditions for the degradation of BPA by a composite catalyst, and improves the utilization of the light energy of TiO_2.

2. Results and Discussion

2.1. Characterization of rGO–P25

Representative Scanning Electron Microscope (SEM) images of pure P25 and 1% rGO–TiO_2 composite photocatalyst with ethanol as solvent are shown in Figure 1a,b, respectively. As shown in Figure 1, the pure P25 with strong agglomeration becomes dispersed when the graphene is added, and the graphene sheet is interspersed between the P25 molecules, forming some rGO–P25 platelets [12,39]. This structure can produce a good deal of surface defect sites, which are beneficial for improving photocatalytic performance [40]. The morphology and structure of 1% rGO–P25 composite photocatalyst are further studied using TEM (Transmission electron microscope), as shown in Figure 1c,d [41]. There is a direct interaction between TiO_2 nanoparticles and rGO sheets, which can prevent the re-aggregation of rGO sheets [42]. According to the HRTEM (High Resolution Transmission Electron Microscope) image (Figure 1d), the TiO_2 particles have a well-resolved lattice feature, where there are lattice spacings of 0.35 nm and 0.24 nm, corresponding to the (101) and (004) approximately [3,43]. Anatase TiO_2 with dominant (101) facets displays high photoactivity because of $O_2^{\bullet-}$ on the composite photocatalyst surface [44].
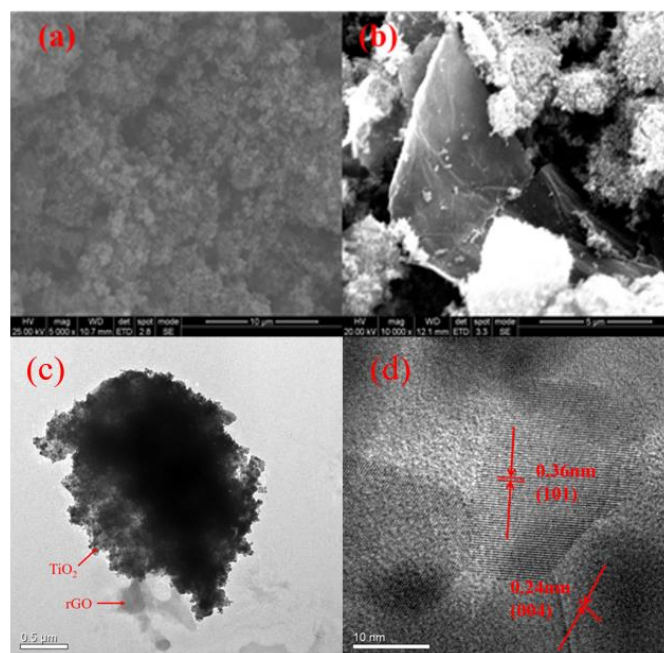
Figure 1. Scanning Electron Microscope (SEM) images of (**a**) pure P25; (**b**) 1% reduced graphene oxide-titanium dioxide photocatalyst (rGO–TiO$_2$) composite photocatalyst with ethanol as solvent; (**c**) TEM micrographs of 1% rGO–P25 and (**d**) HRTEM image of 1% rGO–P25.

Powder XRD (X-ray diffraction) patterns of pure P25, hydrothermal P25 with water as a solvent, hydrothermal P25 with water as well as ethanol (water:ethanol = 2:1) as a solvent and 1% rGO–TiO$_2$ composite photocatalyst with ethanol as solvent are shown in Figure 2a. Compared with peaks of other photocatalysts, the peak of attention at 25.4° of pure P25, which is attributed to (101) facet of anatase TiO$_2$, is lower. This indicates that the proportion of rutile of processed P25 is higher than that of pure P25. After the hydrothermal reaction, part of anatase TiO$_2$ is converted into rutile TiO$_2$ which has a narrower bandgap and a larger absorption range.

Figure 2b shows the FTIR (Fourier Transform infrared spectroscopy) spectra of pure P25, 1%, 3%, and 5% rGO–P25, in the range 400–4000 cm^{-1}. In the FTIR spectrum of pure P25, the representative absorption peaks appear at 3421 (O–H), 1620 (C=C), 1404 (C–OH), and 652 cm^{-1} (Ti–O–Ti) [45–47], respectively. By observing the curve of 1%, 3%, and 5% rGO–P25, it is obvious that the Ti–O–Ti absorption peak was weakened in composite catalysts; this may be the result of the combination of TiO$_2$ and graphene. Furthermore, the observed enhancement of the absorption band at 1621 cm^{-1} could be attributable to skeletal vibration of the graphene [48]. The presence of GO in the 1% rGO–P25 composite catalyst was confirmed by these results [49].

The UV-vis absorption spectra of pure P25 and 1% rGO–P25 photocatalysts are shown in Figure 2c. It is seen that there is similar optical absorption in the range of 250–800 nm of these photocatalysts. However, with the increase of rGO content, photocatalysts cause a redshift of the absorption edge. The reason of this shift is the reducing reflection of light by the presence of carbon [50] and a narrowing of the bandgap of TiO$_2$, which is attributed to chemical bonding between the P25 and graphene [51–53]. The bandgap of pure P25 and 1% rGO–P25 can be calculated according to Equation (1):

$$E_g = 1240/\lambda_g \tag{1}$$

where E_g is the bandgap energy, and λ_g is the absorption edge of the photocatalyst. The absorption edge of pure P25 and 1% rGO–P25 are approximately 423 and 463 nm, respectively. The bandgap of pure P25 and 1% rGO–P25 can be calculated as 2.93 and 2.68 eV, respectively. The addition of rGO

narrows the bandgap of the photocatalyst. This conclusion can explain that both pure P25 and 1% rGO–P25 have the ability to catalytically degrade BPA under visible light [43].
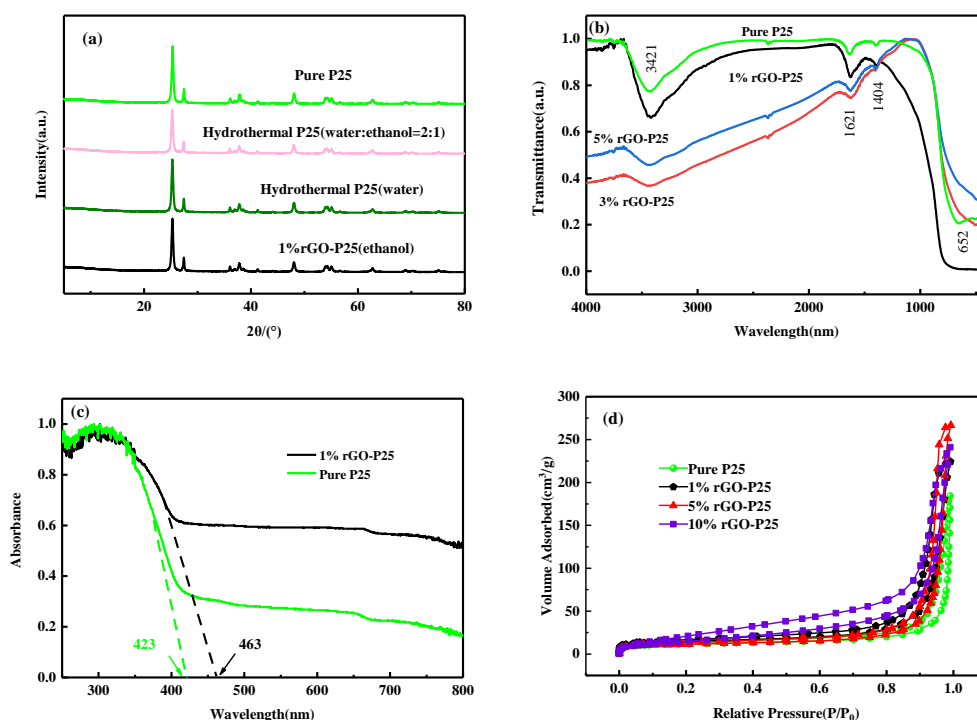
Figure 2. (**a**) XRD patterns of 4 photocatalysts; (**b**) FTIR spectra of pure P25, 1%, 3%, and 5% rGO–P25; (**c**) UV–vis diffuse reflectance spectra of pure P25 and 1% rGO–P25; (**d**) Nitrogen adsorption-desorption isotherms of P25, 1%, 5%, and 10% rGO–P25.

The nitrogen adsorption-desorption isotherms of P25and 1, 5, 10% rGO–P25 are shown in Figure 2d and Table 1. The BET (Brunauer–Emmett–Teller method)surface areas of the pure P25 and 1% rGO–P25 composites are 41.628 and 52.174 m^2/g, respectively. 1% rGO–P25 with the higher specific surface area can offer more active surface sites and photocatalytic reaction centers [54]. It can enhance photocatalytic performance, and this view is confirmed in the following photocatalytic experiments.

**Table 1.** The pore parameters and specific surface area of pure P25, 1%, 5%, and 10% rGO–P25.

Sample	BET (m^2/g)	TPA (mL/g)	d_{mean} (nm)
Pure P25	41.628	0.2717	26.111
1% rGO–P25	52.174	0.3421	26.224
5% rGO–P25	40.816	0.4058	39.729
10% rGO–P25	44.581	0.3685	33.063

2.2. The Catalytic Properties of rGO–P25 under Ultraviolet Light

Figure 3 shows the degradation of BPA under ultraviolet (λ = 350 nm) with different rGO–P25 photocatalysts, which contain different solvents and different contents of rGO.

It can be seen from Figure 3 that under the condition of photocatalysis for 90 min, both rGO–P25 composite catalyst with GO content of 1% or 5% and hydrothermal P25 can remove almost all BPA. The photocatalytic effect on the degradation of BPA with 10% rGO–TiO$_2$ was significantly lower than that of other rGO catalysts. Compared to hydrothermal P25, the presence of rGO did not increase the degradation efficiency but reduced it.

Regarding solvents, there was more of a catalytic effect from water and ethanol (water:ethanol = 2:1) as a solvent than the with water only as a solvent.
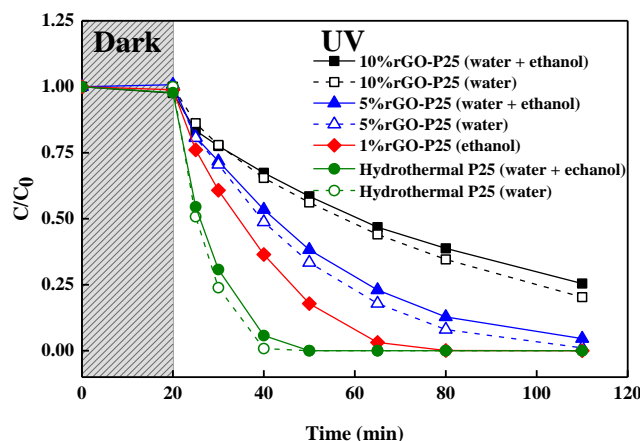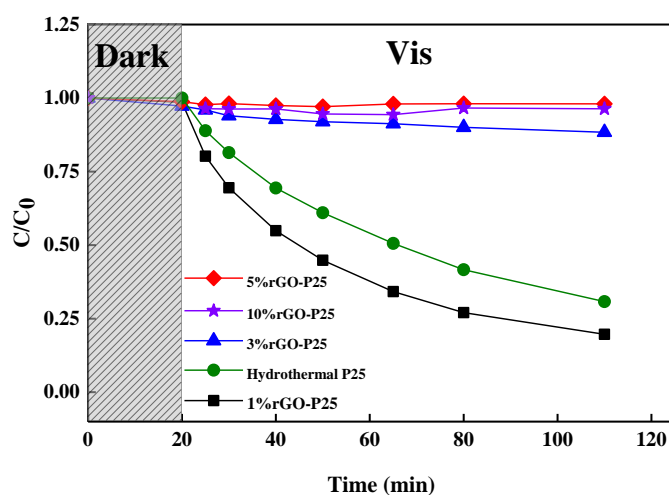
Figure 3. Effect of solvents and contents of rGO on bisphenol A (BPA) degradation by rGO–P25 under UV-light irradiation (BPA concentration = 0.01 mol/L, catalyst dosage = 0.5 g/L, volume of the solution = 100 mL, λ = 350 nm, ten tubes).

2.3. rGO–P25 Photocatalyst Degrades Bisphenol A under Visible Light

2.3.1. The Most Efficient Photocatalyst

Since a variety of composite photocatalysts with different solvents and different rGO contents have been made, it is necessary to select one of the most efficient catalysts under visible light irradiation. Through the experiments, 10%, 5%, 3% rGO–P25, as well as hydrothermal P25 photocatalysts with water as a solvent, and 1% rGO–P25 composite catalyst with ethanol as solvent were selected as competitors that were used for photocatalytic degradation of BPA under the same conditions. The experimental results are shown in Figure 4.
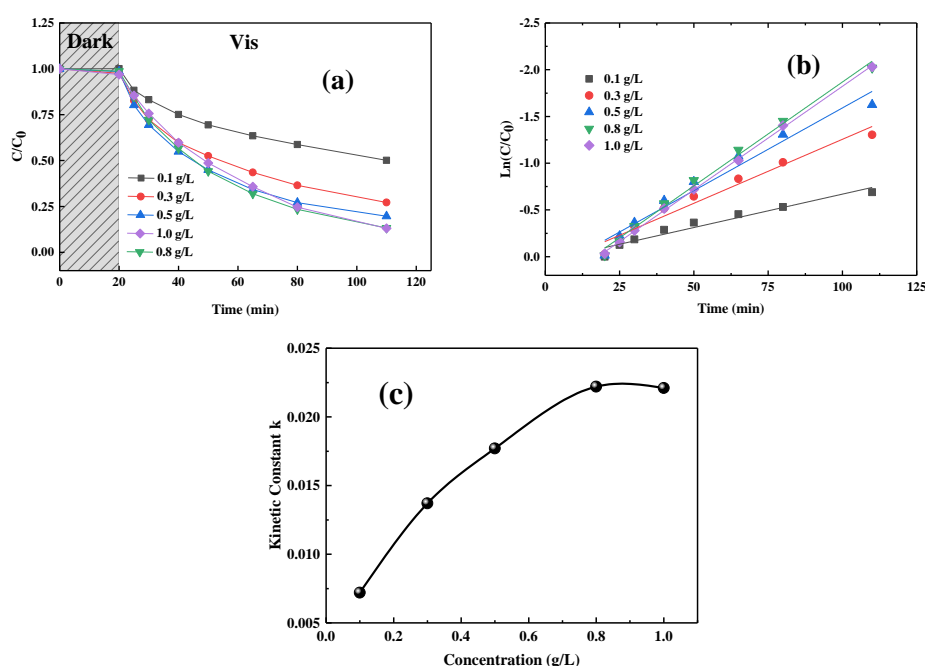

Figure 4. Effect of contents of rGO on BPA degradation by rGO–P25 under visible light irradiation (BPA concentration = 0.01 mol/L, catalyst dosage = 0.5 g/L, volume of the solution = 100 mL, λ = 420 nm, 10 tubes).

From Figure 4, 1% rGO–P25 composite photocatalyst had the best photocatalytic activity when the catalytic system is exposed to visible light (λ = 420 nm). Therefore 1% rGO–P25 was used to research the influence of other factors on photocatalytic activity. In combination with Figure 2d, 1% rGO–P25 had the largest surface area, which is one of the reasons why 1% rGO–P25 had the best photocatalytic efficiency. Pure P25 and 5% and 10% rGO–P25 have a similar specific surface area. Because of the addition of rGO, the color of the catalyst becomes darker to shield the light, which reduces the catalytic efficiency.
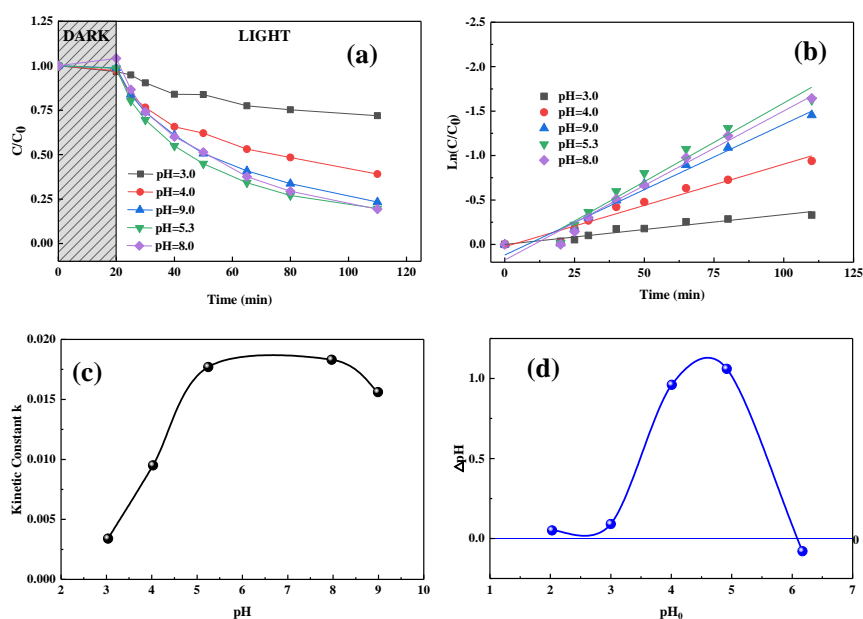
2.3.2. Effect of Catalyst Concentration

The effect of rGO–P25 concentration on catalytic activity is shown in Figure 5. 0.8 g/L was the optimal concentration for photocatalytic degradation of BPA. When the catalyst concentration went from 0.1 to 0.8 g/L, the degradation rate of BPA increased accordingly. The main reason is that as the concentration of the rGO–P25 photocatalyst increased, the active sites of adsorbed contaminants and the e^-/h^+ pair increase accordingly [55]. When the catalyst concentration rose to 1.0 g/L, too much black composite photocatalyst had a shielding effect on light, blocking the progress of the photocatalytic reaction [43]. Therefore, the effect of degrading BPA is decreased. In order to obtain maximum test efficiency and with considerations to save catalysts, the experimental photocatalyst concentration was set to 0.5 g/L.

Figure 5. Effect of the concentration of 1% rGO–P25 on BPA degradation under visible light irradiation. (**a**) Curve of C/C$_0$ versus time; (**b**) corresponding ln(C/C$_0$) and time curve; (**c**) first-order kinetic constant curve of k versus catalyst concentration (BPA concentration = 0.01 mol/L, volume of the solution = 100 mL, λ = 420 nm, 10 tubes).

2.3.3. Effect of Solution pH

The pH of the solution affected the surface properties of the catalyst, and also had an effect on the form of BPA in the solution, which affected the photocatalytic degradation of BPA. The pH of the solution was adjusted to 3.0, 4.0, 8.0, and 9.0, and the photocatalytic activity of the rGO–P25 photocatalyst for degrading BPA at different pH values was investigated. The results are shown in Figure 6.

Figure 6. Effect of solution pH on BPA degradation under visible light irradiation. (**a**) curve of C/C_0 versus time; (**b**) corresponding $\ln(C/C_0)$ and time curve; (**c**) first-order kinetic constant curve of k versus catalyst concentration (BPA concentration = 0.01 mol/L, catalyst dosage = 0.5 g/L, volume of the solution = 100 mL, λ = 420 nm, 10 tubes); and (**d**) isoelectric point of 1% rGO–P25 composite photocatalyst.

In order to clarify the reason why the catalytic ability changes with the solution pH, the isoelectric point of 1% rGO–P25 is also obtained (Figure 6d).

At a certain pH value, a zero potential appears on the surface of the metal oxide. This point is also called Zero Point Charge, which is called zero points, and the corresponding pH is called pH_{zpc}. When the solution pH < pH_{zpc}, the surface of the oxide is positively charged, and vice versa. Taking pH_0 as the abscissa and ΔpH as the ordinate, the curve intersecting the horizontal axis is the isoelectric point of the catalyst. As shown in Figure 6d, the isoelectric point of 1% rGO–P25 was about 6, indicating that when the solution pH was about 6.0, the surface of the catalyst was electrically neutral, and 1% rGO–P25 was positively charged.

It can be seen from Figure 6 that when the pH of the solution is 3.0, the effect of degrading BPA by rGO–P25 photocatalyst was the worst; when the pH of the solution was 5.0–8.0, BPA could be degraded by 80% in 90 min; the degradation effect is better.

If the pH of the solution is greater than the pKa value of 9.58 of BPA, BPA exists mainly in the ionic state in the aqueous phase. When the pH of the solution is less than 6.0, BPA exists mainly in the form of molecular state, and contacts with the catalyst by van der Waals force mainly. H^+ in the solution consumes e^-, reducing the formation of $O_2^{\bullet-}$, which reduces the catalytic capacity of rGO–P25. During the experiment, when the pH of the solution was greater than 8.0, there was be electrostatic repulsion between rGO–P25 photocatalyst with a negatively charged surface, and the negative ions dissociated from BPA, which reduced the adsorption of BPA by the catalyst, resulting in the degenerate of degradation effect.

2.4. Degradation of Bisphenol A under Different Light Sources of the rGO–P25 Photocatalyst

In order to apply the experimental conclusions to the actual situation, a group of experiments was carried out under the illumination of sunlight and LED lamps. The experimental results are shown in Figure 7.
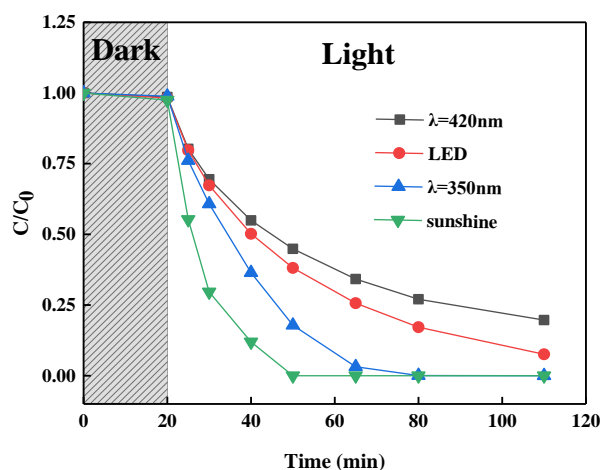
Figure 7. The relationship between C/C_0 and t of the effect of different light sources on the photocatalytic activity of 1% rGO–P25 photocatalyst (catalyst concentration 0.5 g/L, the initial concentration of BPA is 0.01 mol/mL, solution volume is 100 mL).

Figure 7 shows the result that BPA is completely degraded in 90 min under sunlight illumination; even more catalytically than under ultraviolet and visible light. This result can be extended to practical applications and provides a good theoretical basis.

A comparison of the catalytic efficiencies of different kinds of photocatalysts in sunlight is shown in Table 2. As seen from Table 2, 1% rGO–P25 in this work degraded BPA completely with 30 min towards the photocatalytic degradation under sunlight. Among the materials with a degradation rate of more than 95%, 1% rGO–P25 had the shortest time and the highest degradation rate. In almost the same time, 1% rGO–P25 could completely degrade the target pollutants, so it had higher degradation efficiency.

Table 2. Comparison of catalytic efficiency of different photocatalysts under sunlight.

Photocatalyst	Pollution	% Degradation	Time (min)	Light Source	Reference
1% rGO–P25	BPA	100	30	Sunlight	This Work
Cu_2ZnSnS_4	Phthalic acid	56	240	Sunlight	[56]
NiO	MB	94	120	Sunlight	[57]
Cot–g–Si/Ag@ZnO	RhB	98	40	the Xenon Lamp	[58]
$Ni_{0.6}Co_{0.4}O$	MB	95	50	Sunlight	[59]
RGO–TiO_2	Cr	90	100	Simulated Sunlight	[60]
pumice-PSCT	MB	60	30	Simulated Sunlight	[61]
MoS_2/TiO_2	MB	90	90	the Xenon Lamp	[62]
15% BiOBr/TiO_2	CIP	100	180	Sunlight	[63]
Fe/N/S–TiO_2	4-chlorophenol	100	180	Simulated Sunlight	[64]

2.5. Enhancement Mechanism of rGO–P25 Photocatalytic Activity

There are three mechanisms of action of photocatalyst at the photocatalytic reaction mechanism diagram of TiO_2 shown in Figure 8. Firstly, the photocatalyst occupied h^+ to prevent photogenerated electrons from falling back to the valence band. Secondly, $O_2^{\bullet-}$ produced by photocatalyst and oxygen molecules worked. Thirdly, the final product of strong oxidative •OH worked.
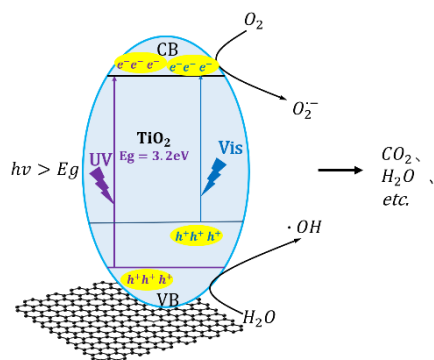
Figure 8. Photocatalytic reaction mechanism.

In order to explore the photocatalytic mechanism of the rGO–P25 composite photocatalyst, this experiment uses an inhibitor to study what mechanism plays a major role. There are five inhibitors, among which: (1) Potassium iodide (KI) and Ethylenediaminetetraacetic acid (EDTA) can occupy h^+ [65]; (2) P-Benzoquinone can capture $O_2^{\bullet-}$ [66]; (3) Methanol and tert-butanol can capture $\bullet OH$ [67].

Under the same conditions, the above five inhibitors were added to the reaction system to make a comparison experiment of 1 mM and 5 mM. The results are shown in Figure 9.
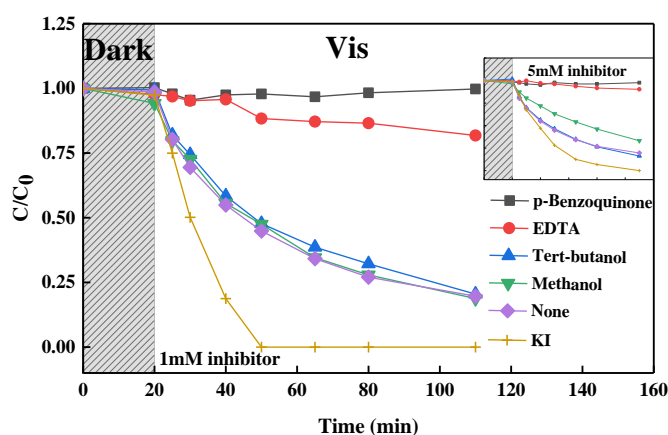
Figure 9. The relationship between C/C_0 and t of the effect of the inhibitor on the photocatalytic activity of rGO–P25 photocatalyst. (visible wavelength 420 nm, 10 tubes, catalyst concentration 0.5 g/L, initial concentration of BPA 0.01 mol/mL, inhibitor concentration is 1 mol/mL, solution volume is 100 mL).

For comparison, the catalytic curve without inhibitor was added in Figure 9. As shown in Figure 9, In the catalytic system in which p-benzoquinone and EDTA were added, BPA was hardly degraded, indicating that they had a very strong inhibitory effect on the photocatalyst. Although methanol and tert-butanol have the effect of capturing hydroxyl radicals, the inhibitory effect was not obvious, and the addition of KI promoted the photocatalytic reaction.

In the photocatalytic reaction of rGO–P25 composite photocatalyst, the active free radical that played a major role was $O_2^{\bullet-}$, and the importance of the three mechanisms affecting the catalytic effect of $O_2^{\bullet-}$ was most important, $\bullet OH$ second, h^+ hole third. The different inhibitory effects of EDTA and KI on the composite catalyst need further study.

3. Materials and Methods

3.1. Materials, Reagents, and Instruments

P25 was purchased from Degussa Chemical Co., Ltd. (Frankfurt, Germany). Graphite powder; analytic purity (99.9%) reagents KI, $C_{10}H_{14}N_2Na_2O_8$, NaCl were purchased from Sinopharm Chemical

Reagent Co., Ltd. (Shanghai, China); analytic purity (99.9%) reagents $NaNO_3$, H_2SO_4, H_3PO_4, $C_4H_{10}O$, $KMnO_4$, CH_3OH, H_2O_2, and ethanol were purchased from Nanjing Chemical Reagent Co., Ltd. (Nanjing, Jiangsu, China). All the Chemical reagents were used directly without further purification before utilization.

The light sources used in the experiment were: lamps (ten, λ = 350 nm and λ = 420 nm, Rayonet, purchased from Southern New England Ultraviolet, Bradford, CT, USA), LED lights (HC-BLZM, purchased from High Glass Group, Guangdong, China), and sunlight.

3.2. Method for Preparing Graphene

Graphene oxide (GO) was prepared following the modified Hummers method [68].

The iron stand was set up, and the flask was set up on the iron stand. The flask was placed in an ice-water bath below 278 K. 4 g of graphite powder, 2 g of $NaNO_3$ were weighed and added to the bottom of the flask in order, and then 100 mL of 98% H_2SO_4 was measured into the flask, which was stirred continuously for 30 min. During mixing, the mixture in the flask became dark green. Then 14 g of $KMnO_4$ was weighed and slowly added into the flask in batches within 30 min; this system was stirred at 308 K for 2 h, at which time the mixture in the flask turned dark brown. Then 200 mL of ultrapure water was added, and the temperature was increased to 368 K during the addition of water, stirring continuously for 3–5 min. Subsequently, 20 mL of H_2O_2 (30%) was added to react with the remaining $KMnO_4$, then 600 mL of ultrapure water was added until there were no bubbles generated, and stirring was continued, at which time the mixture turned yellow.

After 30 min, the flask was taken out, the material was washed with a large amount of hot water (333–343 K), and centrifuged until the graphene was swollen, and the pH of the supernatant was 7.0.

The centrifuge speed was set to 7200 R/min, the rate of 5, 5 min each time.

3.3. Synthesis of the rGO Decorated P25 Microspheres

In this experiment, rGO–P25 photocatalyst was prepared by the hydrothermal method [69]. There were 9 kinds of composite catalysts with different contents of graphene or specific solvents. The mass of graphene was 1% of the mass of P25, and ethanol was used as a solvent. 14 mg of rGO was weighed and added into a 250 mL beaker, then 200 mL of absolute ethanol was added as a solvent. Subsequently, while stirring, 1.4 g of P25 was slowly added in portions, and after all the addition, the ultrasonication and stirring were continued to disperse P25 in the solution completely. Next, the mixture was poured into a Teflon bottle for hydrothermal reaction, keeping at 453 K for 12 h. After cooling, the hydrothermally reacted product was taken out and washed with pure water, drying the catalyst product at 387 K. The graphene content and solvent of other catalysts were shown in Table 3, and the preparation method is the same as the 1% rGO–P25.

Table 3. The graphene content and solvent of other catalysts.

Solvent	Pure Water:Ethanol = 2:1				Pure Water			
Graphene content	10%	5%	3%	0	10%	5%	3%	0
Hydrothermal temperature				393 K				

3.4. Characterization

The X-ray diffraction (XRD) patterns were obtained by Philips (Amsterdam, The Netherlands) X'pert PRO SUPER (Cu-Ka irradiation, λ = 0.15406 nm, 40 kV, 30 mA, 5°–80°, 5°/min). The morphologies and microstructures of materials were observed by scanning electron microscopy (SEM, Quanta 200, FEI, Hillsboro, OR, USA), as well as transmission electron microscope (TEM), and high-resolution TEM (HRTEM, JEM2011, JEOL, Akishima, Japan). The Ultraviolet-visiable diffuse reflectance spectra (UV–vis DRS) were got with Hitachi UH-4150 UV–vis spectrophotometer. The molecular structure of these materials was analyzed using TENSOR 37Fourier transform infrared (FTIR,

BRUKER, Germany) spectroscopy, and spectral normalization was achieved during data processing. The Brunauer–Emmett–Teller (BET) surface area was collected on a BELSORP-miniII volumetric gas sorption instrument (MicrotracBEL, Tokyo, Japan).

3.5. Photocatalytic Activity

According to the preset volume, photocatalyst with a concentration of 0.5 g/L was added to the quartz cup (200 mL), and the catalyst was completely dispersed in water by ultrasonication for 30 min. Then, the target concentration of BPA was added, and the mixed solution was placed in a light reaction box, keeping it in the dark state to be stirred. The adsorption time was set to 20 min. The first sample (about 1.5 mL per sample) was taken before adsorption; the second sample was taken after adsorption, then lights were turned on.

After the adsorption was completed, the lamp tube was selected according to the experimental setting, the light source reaction box was turned on, the timing was started, and each sample was taken at t = 5, 10, 20, 30, 45, 60, 90 min. There were 9 samples in total. The BPA solution was separated from the catalyst with a syringe and filter, and peak area was measured by liquid chromatography (UltiMate 3000, Thermo-Dionex Corporation, Waltham, MA, USA). The specification of the LC column was via Syncronis C18, (Dim.(mm) 150*4.6).

4. Conclusions

In this work, rGO–P25 composite photocatalyst was synthesized by hydrothermal method. The synthesis of rGO–P25 solved the problems of TiO_2 with large bandgap energy, low adsorption capacity for pollutants, and an easily compoundable electron-hole pair. From the characterization results, the crystal phase of TiO_2 changed, and the specific surface area of the photocatalyst increased because of the addition of rGO. The results of photocatalytic experiments showed that 0.5 g/L 1% rGO–P25 was the most suitable to degrade BPA when pH was 5–8, and the degradation rate could reach 100% in 30 min under sunlight. Finally, the mechanism analysis showed that $O_2^{\bullet-}$ played a major role in the reaction mechanism of 1% rGO–P25. The results of this study showed that 1% rGO–TiO_2 has not only high catalytic efficiency, but also wide applicability.

Author Contributions: Conceived the project and writing—original draft preparation, F.Y., X.B.; manipulation, data analysis and drawing, X.B., C.Y.; supervision, review and editing, L.X., J.M.

Conflicts of Interest: The authors declare no conflict of interest.

References

1. Zerjav, G.; Djinovic, P.; Pintar, A. TiO₂-Bi₂O₃/(BiO)_(2)CO₃-reduced graphene oxide composite as an effective visible light photocatalyst for degradation of aqueous bisphenol A solutions. *Catal. Today* **2018**, *315*, 237–246. [CrossRef]
2. Li, X.; Sun, M.-Z.; Li, X.; Zhang, S.-H.; Dai, L.-T.; Liu, X.-Y.; Zhao, X.; Chen, D.-Y.; Feng, X.-Z. Impact of low-dose chronic exposure to Bisphenol A (BPA) on adult male zebrafish adaption to the environmental complexity: Disturbing the color preference patterns and reliving the anxiety behavior. *Chemosphere* **2017**, *186*, 295–304. [CrossRef] [PubMed]
3. Zhang, Y.; Cui, W.Q.; An, W.J.; Liu, L.; Liang, Y.H.; Zhu, Y.F. Combination of photoelectrocatalysis and adsorption for removal of bisphenol A over TiO₂-graphene hydrogel with 3D network structure. *Appl. Catal. B Environ.* **2018**, *221*, 36–46. [CrossRef]
4. Ran, P.; Jiang, L.; Li, X.; Zuo, P.; Li, B.; Li, X.J.; Cheng, X.Y.; Zhang, J.T.; Lu, Y.F. Redox shuttle enhances nonthermal femtosecond two-photon self-doping of rGO-TiO₂-x photocatalysts under visible light. *J. Mater. Chem. A* **2018**, *6*, 16430–16438. [CrossRef]

5. Sharma, A.; Lee, B.K. Rapid photo-degradation of 2-chlorophenol under visible light irradiation using cobalt oxide-loaded TiO$_2$/reduced graphene oxide nanocomposite from aqueous media. *J. Environ. Manag.* **2016**, *165*, 1–10. [CrossRef]

6. Zerjav, G.; Arshad, M.S.; Djinovic, P.; Junkar, I.; Kovac, J.; Zavasnik, J.; Pintar, A. Improved electron-hole separation and migration in anatase TiO$_2$ nanorod/reduced graphene oxide composites and their influence on photocatalytic performance. *Nanoscale* **2017**, *9*, 4578–4592. [CrossRef]

7. Yang, L.; Li, Z.; Jiang, H.; Jiang, W.; Su, R.; Luo, S.; Luo, Y. Photoelectrocatalytic oxidation of bisphenol A over mesh of TiO$_2$/graphene/Cu$_2$O. *Appl. Catal. B Environ.* **2016**, *183*, 75–85. [CrossRef]

8. Cruz-Ortiz, B.R.; Hamilton, J.W.J.; Pablos, C.; Diaz-Jimenez, L.; Cortes-Hernandez, D.A.; Sharma, P.K.; Castro-Alferez, M.; Fernandez-Ibanez, P.; Dunlop, P.S.M.; Byrne, J.A. Mechanism of photocatalytic disinfection using titania-graphene composites under UV and visible irradiation. *Chem. Eng. J.* **2017**, *316*, 179–186. [CrossRef]

9. Lee, S.-Y.; Park, S.-J. TiO$_2$ photocatalyst for water treatment applications. *J. Ind. Eng. Chem.* **2013**, *19*, 1761–1769. [CrossRef]

10. Mohamed, R.M.; Ismail, A.A.; Kadi, M.W.; Bahnemann, D.W. A comparative study on mesoporous and commercial TiO$_2$ photocatalysts for photodegradation of organic pollutants. *J. Photochem. Photobiol. A Chem.* **2018**, *367*, 66–73. [CrossRef]

11. Xing, Z.; Zhang, J.; Cui, J.; Yin, J.; Zhao, T.; Kuang, J.; Xiu, Z.; Wan, N.; Zhou, W. Recent advances in floating TiO$_2$-based photocatalysts for environmental application. *Appl. Catal. B Environ.* **2018**, *225*, 452–467. [CrossRef]

12. Cruz, M.; Gomez, C.; Duran-Valle, C.J.; Pastrana-Martinez, L.M.; Faria, J.L.; Silva, A.M.T.; Faraldos, M.; Bahamonde, A. Bare TiO$_2$ and graphene oxide TiO$_2$ photocatalysts on the degradationof selected pesticides and influence of the water matrix. *Appl. Surf. Sci.* **2017**, *416*, 1013–1021. [CrossRef]

13. Zhao, H.; Chen, S.; Quan, X.; Yu, H.; Zhao, H. Integration of microfiltration and visible-light-driven photocatalysis on g-C$_3$N$_4$ nanosheet/reduced graphene oxide membrane for enhanced water treatment. *Appl. Catal. B Environ.* **2016**, *194*, 134–140. [CrossRef]

14. Pu, S.Y.; Zhu, R.X.; Ma, H.; Deng, D.L.; Pei, X.J.; Qi, F.; Chu, W. Facile in-situ design strategy todisperse TiO$_2$ nanoparticles on graphene for the enhanced photocatalytic degradation of rhodamine 6G. *Appl. Catal. B Environ.* **2017**, *218*, 208–219. [CrossRef]

15. Lai, C.; Wang, M.M.; Zeng, G.M.; Liu, Y.G.; Huang, D.L.; Zhang, C.; Wang, R.Z.; Xu, P.; Cheng, M.; Huang, C.; et al. Synthesis of surface molecular imprinted TiO$_2$/graphene photocatalyst and its highly efficient photocatalytic degradation of target pollutant under visible light irradiation. *Appl. Surf. Sci.* **2016**, *390*, 368–376. [CrossRef]

16. Wang, S.; Li, D.; Sun, C.; Yang, S.; Guan, Y.; He, H. Synthesis and characterization of g-C$_3$N$_4$/Ag$_3$VO$_4$ composites with significantly enhanced visible-light photocatalytic activity for triphenylmethane dye degradation. *Appl. Catal. B Environ.* **2014**, *144*, 885–892. [CrossRef]

17. D'Amato, C.A.; Giovannetti, R.; Zannotti, M.; Rommozzi, E.; Ferraro, S.; Seghetti, C.; Minicucci, M.; Gunnella, R.; Di Cicco, A. Enhancement of visible-light photoactivity by polypropylene coated plasmonic Au/TiO$_2$ for dye degradation in water solution. *Appl. Surf. Sci.* **2018**, *441*, 575–587. [CrossRef]

18. Lin, L.; Wang, H.; Xu, P. Immobilized TiO$_2$-reduced graphene oxide nanocomposites on optical fibers as high performance photocatalysts for degradation of pharmaceuticals. *Chem. Eng. J.* **2017**, *310*, 389–398. [CrossRef]

19. Qi, K.Z.; Cheng, B.; Yu, J.G.; Ho, W.K. A review on TiO$_2$-based Z-scheme photocatalysts. *Chin. J. Catal.* **2017**, *38*, 1936–1955. [CrossRef]

20. Doong, R.A.; Liao, C.Y. Enhanced visible-light-responsive photodegradation of bisphenol A by Cu, N-codoped titanate nanotubes prepared by microwave-assisted hydrothermal method. *J. Hazard. Mater.* **2017**, *322*, 254–262. [CrossRef] [PubMed]

21. He, X.J.; Aker, W.G.; Pelaez, M.; Lin, Y.F.; Dionysiou, D.D.; Hwang, H.M. Assessment of nitrogen-fluorine-codoped TiO$_2$ under visible light for degradation of BPA: Implication for field remediation. *J. Photochem. Photobiol. A Chem.* **2016**, *314*, 81–92. [CrossRef]

22. Chen, C.; Zhang, Y.; Zeng, J.; Zhang, F.; Zhou, K.; Bowen, C.R.; Zhang, D. Aligned macroporous TiO$_2$/chitosan/reduced graphene oxide (rGO) composites for photocatalytic applications. *Appl. Surf. Sci.* **2017**, *424*, 170–176. [CrossRef]

23. Faraldos, M.; Bahamonde, A. Environmental applications of titania-graphene photocatalysts. *Catal. Today* **2017**, *285*, 13–28. [CrossRef]

24. Wan, J.; Wei, M.; Hu, Z.; Peng, Z.; Wang, B.; Feng, D.; Shen, Y. Ternary composites of TiO_2 nanotubes with reduced graphene oxide (rGO) and meso-tetra (4-carboxyphenyl) porphyrin for enhanced visible light photocatalysis. *Int. J. Hydrog. Energy* **2016**, *41*, 14692–14703. [CrossRef]

25. Liu, Y.; Zhang, Z.; Hu, R. Synthesis of three-dimensional hierarchically porous reduced graphene oxide–TiO_2 nanocomposite for enhanced hydrogen storage. *Ceram. Int.* **2018**, *44*, 12458–12465. [CrossRef]

26. Szabó, T.; Veres, Á.; Cho, E.; Khim, J.; Varga, N.; Dékány, I. Photocatalyst separation from aqueous dispersion using graphene oxide/TiO_2 nanocomposites. *Colloids Surf. A Physicochem. Eng. Asp.* **2013**, *433*, 230–239. [CrossRef]

27. Chen, L.; Li, Y.H.; Chen, L.N.; Li, N.; Dong, C.L.; Chen, Q.; Liu, B.B.; Ai, Q.; Si, P.C.; Feng, J.K.; et al. A large-area free-standing graphene oxide multilayer membrane with high stability for nanofiltration applications. *Chem. Eng. J.* **2018**, *345*, 536–544. [CrossRef]

28. Zhang, L.; Shi, Y.; Wang, L.; Hu, C. AgBr-wrapped Ag chelated on nitrogen-doped reduced graphene oxide for water purification under visible light. *Appl. Catal. B Environ.* **2018**, *220*, 118–125. [CrossRef]

29. Jiang, G.D.; Lin, Z.F.; Chen, C.; Zhu, L.H.; Chang, Q.; Wang, N.; Wei, W.; Tang, H.Q. TiO_2 nanoparticles assembled on graphene oxide nanosheets with high photocatalytic activity for removal of pollutants. *Carbon* **2011**, *49*, 2693–2701. [CrossRef]

30. Wu, H.; Lu, W.; Shao, J.-J.; Zhang, C.; Wu, M.-B.; Li, B.-H.; Yang, Q.-H. pH-dependent size, surface chemistry and electrochemical properties of graphene oxide. *New Carbon Mater.* **2013**, *28*, 327–335. [CrossRef]

31. Bi, H.C.; Xie, X.; Yin, K.B.; Zhou, Y.L.; Wan, S.; He, L.B.; Xu, F.; Banhart, F.; Sun, L.T.; Ruoff, R.S. Spongy Graphene as a Highly Efficient and Recyclable Sorbent for Oils and Organic Solvents. *Adv. Funct. Mater.* **2012**, *22*, 4421–4425. [CrossRef]

32. Yu, X.Q.; Lin, D.M.; Li, P.; Su, Z.Q. Recent advances in the synthesis and energy applications of TiO_2-graphene nanohybrids. *Sol. Energy Mater. Sol. Cells* **2017**, *172*, 252–269. [CrossRef]

33. Wang, P.; Wang, J.; Wang, X.; Yu, H.; Yu, J.; Lei, M.; Wang, Y. One-step synthesis of easy-recycling TiO_2-rGO nanocomposite photocatalysts with enhanced photocatalytic activity. *Appl. Catal. B Environ.* **2013**, *132*, 452–459. [CrossRef]

34. Seredych, M.; Bandosz, T.J. Effects of Surface Features on Adsorption of SO2 on Graphite Oxide/$Zr(OH)_{(4)}$ Composites. *J. Phys. Chem. C* **2010**, *114*, 14552–14560. [CrossRef]

35. Zhu, C.Z.; Guo, S.J.; Wang, P.; Xing, L.; Fang, Y.X.; Zhai, Y.M.; Dong, S.J. One-pot, water-phase approach to high-quality graphene/TiO_2 composite nanosheets. *Chem. Commun.* **2010**, *46*, 7148–7150. [CrossRef] [PubMed]

36. Han, W.J.; Ren, L.; Gong, L.J.; Qi, X.; Liu, Y.D.; Yang, L.W.; Wei, X.L.; Zhong, J.X. Self-Assembled Three-Dimensional Graphene-Based Aerogel with Embedded Multifarious Functional Nanoparticles and Its Excellent Photoelectrochemical Activities. *ACS Sustain. Chem. Eng.* **2014**, *2*, 741–748. [CrossRef]

37. Simsek, E.B.; Kilic, B.; Asgin, M.; Akan, A. Graphene oxide based heterojunction TiO_2-ZnO catalysts with outstanding photocatalytic performance for bisphenol-A, ibuprofen and flurbiprofen. *J. Ind. Eng. Chem.* **2018**, *59*, 115–126. [CrossRef]

38. Liao, G.; Zhu, D.; Zheng, J.; Yin, J.; Lan, B.; Li, L. Efficient mineralization of bisphenol A by photocatalytic ozonation with TiO_2-graphene hybrid. *J. Taiwan Inst. Chem. Eng.* **2016**, *67*, 300–305. [CrossRef]

39. Jiang, B.J.; Tian, C.G.; Zhou, W.; Wang, J.Q.; Xie, Y.; Pan, Q.J.; Ren, Z.Y.; Dong, Y.Z.; Fu, D.; Han, J.L.; et al. In Situ Growth of TiO_2 in Interlayers of Expanded Graphite for the Fabrication of TiO_2-Graphene with Enhanced Photocatalytic Activity. *Chem. A Eur. J.* **2011**, *17*, 8379–8387. [CrossRef]

40. Ke, J.; Li, X.Y.; Zhao, Q.D.; Liu, B.J.; Liu, S.M.; Wang, S.B. Upconversion carbon quantum dots as visible light responsive component for efficient enhancement of photocatalytic performance. *J. Colloid Interface Sci.* **2017**, *496*, 425–433. [CrossRef]

41. Zhang, J.; Zhang, L.L.; Shi, Y.X.; Xu, G.L.; Zhang, E.P.; Wang, H.B.; Kong, Z.; Xi, J.H.; Ji, Z.G. Anatase TiO_2 nanosheets with coexposed {101} and {001} facets coupled with ultrathin SnS_2 nanosheets as a face-to-face n-p-n dual heterojunction photocatalyst for enhancing photocatalytic activity. *Appl. Surf. Sci.* **2017**, *420*, 839–848. [CrossRef]

42. Štengl, V.; Bakardjieva, S.; Grygar, T.M.; Bludská, J.; Kormunda, M. TiO_2-graphene oxide nanocomposite as advanced photocatalytic materials. *Chem. Cent. J.* **2013**, *7*, 41. [CrossRef] [PubMed]

43. Xu, L.; Yang, L.; Johansson, E.M.J.; Wang, Y.; Jin, P. Photocatalytic activity and mechanism of bisphenol a removal over TiO2-x/rGO nanocomposite driven by visible light. *Chem. Eng. J.* **2018**, *350*, 1043–1055. [CrossRef]

44. Xiong, Z.; Zhao, X.S. Nitrogen-Doped Titanate-Anatase Core–Shell Nanobelts with Exposed {101} Anatase Facets and Enhanced Visible Light Photocatalytic Activity. *J. Am. Chem. Soc.* **2012**, *134*, 5754–5757. [CrossRef] [PubMed]

45. Xu, J.; Wang, L.; Zhu, Y. Decontamination of Bisphenol A from Aqueous Solution by Graphene Adsorption. *Langmuir* **2012**, *28*, 8418–8425. [CrossRef] [PubMed]

46. Liu, W.; Cai, J.; Ding, Z.; Li, Z. TiO2/RGO composite aerogels with controllable and continuously tunable surface wettability for varied aqueous photocatalysis. *Appl. Catal. B Environ.* **2015**, *174–175*, 421–426. [CrossRef]

47. Ali, M.H.H.; Al-Afify, A.D.; Goher, M.E. Preparation and characterization of graphene—TiO2 nanocomposite for enhanced photodegradation of Rhodamine-B dye. *Egypt. J. Aquat. Res.* **2018**, *44*, 263–270. [CrossRef]

48. Rommozzi, E.; Zannotti, M.; Giovannetti, R.; D'Amato, C.A.; Ferraro, S.; Minicucci, M.; Gunnella, R.; Di Cicco, A. Reduced Graphene Oxide/TiO2 Nanocomposite: From Synthesis to Characterization for Efficient Visible Light Photocatalytic Applications. *Catalysts* **2018**, *8*, 598. [CrossRef]

49. Pan, X.; Zhao, Y.; Liu, S.; Korzeniewski, C.L.; Wang, S.; Fan, Z. Comparing Graphene-TiO2 Nanowire and Graphene-TiO2 Nanoparticle Composite Photocatalysts. *ACS Appl. Mater. Interfaces* **2012**, *4*, 3944–3950. [CrossRef]

50. Khalid, N.R.; Ahmed, E.; Hong, Z.L.; Ahmad, M. Synthesis and photocatalytic properties of visible light responsive La/TiO2-graphene composites. *Appl. Surf. Sci.* **2012**, *263*, 254–259. [CrossRef]

51. Wang, P.F.; Ao, Y.H.; Wang, C.; Hou, J.; Qian, J. Enhanced photoelectrocatalytic activity for dye degradation by graphene-titania composite film electrodes. *J. Hazard. Mater.* **2012**, *223*, 79–83. [CrossRef] [PubMed]

52. Zhang, X.Y.; Li, H.P.; Cui, X.L.; Lin, Y.H. Graphene/TiO2 nanocomposites: Synthesis, characterization and application in hydrogen evolution from water photocatalytic splitting. *J. Mater. Chem.* **2010**, *20*, 2801–2806. [CrossRef]

53. Pu, S.H.; Long, D.B.; Liu, Z.H.; Yang, F.Y.; Zhu, J.M. Preparation of RGO-P25 Nanocomposites for the Photocatalytic Degradation of Ammonia in Livestock Farms. *Catalysts* **2018**, *8*, 189. [CrossRef]

54. Liu, L.; Luo, C.; Xiong, J.; Yang, Z.X.; Zhang, Y.B.; Cai, Y.X.; Gu, H.S. Reduced graphene oxide (rGO) decorated TiO2 microspheres for visible-light photocatalytic reduction of Cr(VI). *J. Alloy. Compd.* **2017**, *690*, 771–776. [CrossRef]

55. Bora, L.V.; Mewada, R.K. Visible/solar light active photocatalysts for organic effluent treatment: Fundamentals, mechanisms and parametric review. *Renew. Sustain. Energy Rev.* **2017**, *76*, 1393–1421. [CrossRef]

56. Hunge, Y.M.; Yadav, A.A.; Liu, S.; Mathe, V.L. Sonochemical synthesis of CZTS photocatalyst for photocatalytic degradation of phthalic acid. *Ultrason. Sonochem.* **2019**, *56*, 284–289. [CrossRef]

57. Ramasami, A.K.; Reddy, M.V.; Balakrishna, G.R. Combustion synthesis and characterization of NiO nanoparticles. *Mater. Sci. Semicond. Process.* **2015**, *40*, 194–202. [CrossRef]

58. Wang, M.L.; Zhang, M.J.; Zhang, M.X.; Aizezi, M.; Zhang, Y.M.; Hu, J.T.; Wu, G.Z. In-situ mineralized robust polysiloxane-Ag@ZnO on cotton for enhanced photocatalytic and antibacterial activities. *Carbohydr. Polym.* **2019**, *217*, 15–25. [CrossRef]

59. Khatri, A.; Rana, P.S. Visible light photocatalysis of methylene blue using cobalt substituted cubic NiO nanoparticles. *Bull. Mater. Sci.* **2019**, *42*, 141. [CrossRef]

60. Shang, H.Y.; Ma, M.; Liu, F.S.; Miao, Z.; Zhang, A.P. Self-Assembled Reduced Graphene Oxide-TiO2 Thin Film for the Enhanced Photocatalytic Reduction of Cr(VI) Under Simulated Solar Irradiation. *J. Nanosci. Nanotechnol.* **2019**, *19*, 3376–3387. [CrossRef]

61. Shao, L.; Liu, H.; Zeng, W.P.; Zhou, C.Y.; Li, D.; Wang, L.; Lan, Y.Q.; Xu, F.G.; Liu, G.S. Immobilized and photocatalytic performances of PDMS-SiO2-chitosan@ TiO2 composites on pumice under simulated sunlight irradiation. *Appl. Surf. Sci.* **2019**, *478*, 1017–1026. [CrossRef]

62. Teng, W.; Wang, Y.M.; Lin, Q.; Zhu, H.; Tang, Y.B.; Li, X.Y. Synthesis of MoS2/TiO2 Nanophotocatalyst and Its Enhanced Visible Light Driven Photocatalytic Performance. *J. Nanosci. Nanotechnol.* **2019**, *19*, 3519–3527. [CrossRef] [PubMed]

63. Rashid, J.; Abbas, A.; Chang, L.C.; Iqbal, A.; Haq, I.U.; Rehman, A.; Awan, S.U.; Arshad, M.; Rafique, M.; Barakat, M.A. Butterfly cluster like lamellar BiOBr/TiO$_2$ nanocomposite for enhanced sunlight photocatalytic mineralization of aqueous ciprofloxacin. *Sci. Total Environ.* **2019**, *665*, 668–677. [CrossRef] [PubMed]

64. Villaluz, F.D.A.; de Luna, M.D.G.; Colades, J.I.; Garcia-Segura, S.; Lu, M.C. Removal of 4-chlorophenol by visible-light photocatalysis using ammonium iron (II) sulfate-doped nano-titania. *Process Saf. Environ. Prot.* **2019**, *125*, 121–128. [CrossRef]

65. Wang, W.; Zhang, L.; An, T.; Li, G.; Yip, H.-Y.; Wong, P.-K. Comparative study of visible-light-driven photocatalytic mechanisms of dye decolorization and bacterial disinfection by B–Ni-codoped TiO$_2$ microspheres: The role of different reactive species. *Appl. Catal. B Environ.* **2011**, *108–109*, 108–116. [CrossRef]

66. Gao, F.; Jiang, J.; Du, L.; Liu, X.; Ding, Y. Stable and highly efficient Cu/TiO$_2$ nanocomposite photocatalyst prepared through atomic layer deposition. *Appl. Catal. A Gen.* **2018**, *568*, 168–175. [CrossRef]

67. Ma, J.; Sun, Y.; Zhang, M.; Yang, M.; Gong, X.; Yu, F.; Zheng, J. Comparative Study of Graphene Hydrogels and Aerogels Reveals the Important Role of Buried Water in Pollutant Adsorption. *Environ. Sci. Technol.* **2017**, *51*, 12283–12292. [CrossRef]

68. Yadav, N.; Lochab, B. A Comparative Study of Graphene Oxide: Hummers, Intermediate and Improved method. *FlatChem* **2019**. [CrossRef]

69. Zhou, K.F.; Zhu, Y.H.; Yang, X.L.; Jiang, X.; Li, C.Z. Preparation of graphene-TiO$_2$ composites with enhanced photocatalytic activity. *New J. Chem.* **2011**, *35*, 353–359. [CrossRef]